Title

Lifshitz Transitions Induced by Temperature and Surface Doping in Type-II Weyl Semimetal Candidate Td-WTe2

Journal

physica status solidi (RRL) - Rapid Research Letters, 11(12)

ISSN

1862-6254

Authors

Zhang, Qihang

Liu, Zhongkai

Sun, Yan

et al.

Publication Date

2017-12-01

DOI

10.1002/pssr.201700209

Peer reviewed

Lifshitz Transitions Induced by Temperature and Surface Doping in Type-II Weyl Semimetal Candidate T_d-WTe_2

Q. Zhang[1], Z. K. Liu[2], Y. Sun[3], H. F. Yang[4,5], J. Jiang[2,4,6], S.-K. Mo[6], Z. Hussain[6], X. F. Qian[7], L. Fu[8], S. H. Yao[9], M. H. Lu[9], C. Felser[3], B. H. Yan[3], Y. L. Chen[1,2,4*] and L. X. Yang[1*],

[1]*State Key Laboratory of Low Dimensional Quantum Physics, Department of Physics and Collaborative Innovation Center of Quantum Matter, Tsinghua University, Beijing 100084, P. R. China*
[2]*School of Physical Science and Technology, ShanghaiTech University, Shanghai 200031, China*
[3]*Max Planck Institute for Chemical Physics of Solids, D-01187 Dresden, Germany*
[4]*Department of Physics, Clarendon Laboratory, University of Oxford Parks Road, Oxford, OX1 3PU, UK*
[5]*Laboratary of Functional materials for Informatics, Shanghai Institute of Microsystem and Information Technology (SIMIT), Chinese Acadamy of Sciences, 865 Changning Road, Shanghai 200050, China*
[6]*Advanced Light Source, Lawrence Berkeley National Laboratory, Berkeley, CA 94720, USA*
[7]*Department of Nuclear Science and Engineering and Department of Materials Science and Engineering, Massachusetts Institute of Technology, Cambridge, MA 02139, USA*
[8]*Department of Physics, Massachusetts Institute of Technology, Cambridge, Massachusetts 02139, USA*
[9]*National Laboratory of Solid State Microstructures, Department of Materials Science and Engineering, Nanjing University, Nanjing, China*

[*] *Email: yulin.chen@physics.ox.ac.uk, lxyang@tsinghua.edu.cn*

Abstract

Transition metal dichalcogenides T_d-XTe_2 (X = W, Mo) have attracted substantial research attention recently not only due to their rich unusual properties (e.g. quantum spin Hall effect in their thin films[1], extremely large and non-saturating magnetoresistance[2] , and temperature induced Lifshitz transition[3], etc.), but also because they can harbour the type-II topological Weyl semimetal (TWS) phase[4-7]. Here, using high resolution angle-resolved photoemission spectroscopy (ARPES) to systematically investigate the electronic structure of T_d-WTe_2, we realized two-stage Lifschitz transitions induced by temperature regulation and surface modification, respectively. We showed a broad agreement between the measured electronic structure at 9 K and our *ab-initio* calculations which suggests a type-II TWS phase at low temperature as favoured by the observation of a significant lattice contraction. Remarkably, we observed a drastic electronic structure evolution showing a large Rashba-like splitting after violent surface modulation, which visualizes the strong spin-orbit coupling in T_d-WTe_2 and provides a promising method to manipulate its electronic structure and physical properties.

Introduction

Topological Weyl semimetals (TWSs) represent a novel topological quantum state recently discovered that is characterized by the existence of bulk Weyl fermions and topological surface Fermi-arcs connecting Weyl points of opposite chirality[8]. Upon their discovery, TWSs have evoked enormous research interests due to their intriguing physical properties and broad application potential[8-16]. Soon after the establishment of the TWS phase in the transition metal mono-pnictide (TMMP) family[17-22], a type-II TWS phase was theoretically proposed in T_d-XTe_2 (M = W, Mo) that violates the Lorentz symmetry[4], thus strongly tilting the bulk Weyl cones to introduce non-vanishing bulk (both electron and hole) Fermi pockets on the Fermi surface (FS) [4-7, 23-29]. Compared to the complicated distribution of 24 Weyl fermions in the TMMPs and their three-dimensional (3D) crystal structures, T_d-XTe_2 not only has much more concise distribution of (4 or 8) Weyl fermions, but also crystallizes into layered structure, thus providing a more promising material basis to design, process and fabricate TWS-based electronic and spintronic devices.

Moreover, besides being recognized as type-II TWSs, T_d-XTe_2 materials are well-known to possess other rich and intriguing physical properties, such as quantum spin Hall effect[1] , non-saturating magnetoresistance[2], strong spin-orbit coupling[30] and temperature induced Lifschitz transition[3]. T_d-XTe_2 family of compounds thus serve as an ideal platform to investigate different emergent properties and their interplay in topological quantum materials. Despite tremendous efforts over the past couple of years, however, the understanding of the detailed electronic properties of T_d-XTe_2 still remains elusive and controversial[23-27, 29, 31, 32]. For example, a complete picture of the 3D electronic structure, a systematic evolution of the electronic structure with external parameters, and a direct visualization of its strong spin-orbit coupling are still essentially lacking.

In this work, by performing systematic high-resolution ARPES measurements, we presented the detailed electronic structure of T_d-WTe_2 and its evolution with k_z momentum, temperature and

surface modification. We were able to realize two-stage Lifshitz transitions induced by both temperature regulation and surface modification. The electronic structure measured at low temperature can be well reproduced by our *ab-initio* calculations under reduced lattice parameters and a significant lattice contraction was observed at low temperatures, which favours a type-II TWS phase as suggested by our *ab-initio* calculations. Remarkably, we observed a drastic electronic structure reconstruction and a large Rashba-like splitting after substantial surface dosing of alkali metal atoms, which directly visualizes the strong spin-orbit coupling effect in T_d-WTe_2. Our work not only is instructive and incentive for the full establishment of the type-II TWS phase in T_d-WTe_2, but also establishes a feasible and controllable method to manipulate the fundamental electronic structure and physical properties of type-II TWSs.

Results

Overall electronic structure of T_d-WTe_2

The crystal structure of T_d-WTe_2 are shown in Fig. 1A. The lattice of T_d-WTe_2 is strongly distorted, forming quasi-one dimensional chains of W atoms along *b* axis and canting Te-W octahedral (T_d phase, see Fig. 1A). With decreasing temperature, the lattice shrinks along all the three lattice axes with a volume expansion coefficient of about 7.2×10^{-5} K^{-1} from our temperature dependent XRD measurements (Fig. 1B**)**. The sharp peaks of the W *4f* and Te *4d* doublets in the core level photoemission spectrum (Fig. 1C) suggest high quality of our T_d-WTe_2 single crystals. The FS mapping over multiple BZs in Fig. 1D confirmed the (001) cleavage and a strongly anisotropic electronic structure of T_d-WTe_2 along the k_x and k_y directions (which is consistent with its orthorhombic crystal structure in Fig. 1A).

According to our *ab-initio* calculations, the type-II TWS phase in T_d-WTe_2 is extremely sensitive to the lattice constant and only exist when the lattice constants are smaller than a = 3.463 Å, b = 6.230 Å and c = 14.00 Å (see Supplementary Information for details). Our temperature

dependent XRD measurements in Fig. 2B suggests that T_d-WTe_2 indeed falls into the predicted type-II TWS phase, in consistence with previous report[4]. The predicted four pairs of Weyl points are present in each BZ at [(±0.037, ±0.220, 0) Å^{-1}, E_F + 55 meV] (W1) and [(±0.056, ±0.220, 0) Å^{-1}, E_F + 70 meV] (W2), respectively, as illustrated in Fig. 1E, F. Due to the strong tilting of the Weyl cones[4], there exist both electron and hole pockets on the FS of T_d-WTe_2 (Fig. 1G**)**, which are connected by the surface Fermi arcs (highlighted by the green thick curve in Fig. 1G (ii)).

Figure 2A demonstrates a 3D intensity plot of the band structure of T_d-WTe_2 measured at 9 K, where we observe strongly anisotropic band structure along $\bar{\Gamma}$-$\bar{Y}$ and $\bar{\Gamma}$-$\bar{X}$. The fine structure of the FS consists of pockets locating near k_y= ± 0.2 Å^{-1} and k_y = ± 0.4 Å^{-1} (Fig. 2B(i), (ii)). The FS pockets are overall very small compared with the BZ, suggesting low carrier density near E_F of T_d-WTe_2. The measured band structures along high-symmetry directions show general agreement with our *ab-initio* calculations under reduced lattice parameters as compared in Fig. 2C ($\bar{Y}$-$\bar{\Gamma}$-$\bar{Y}$) and Fig. 2E ($\bar{X}$-$\bar{\Gamma}$-$\bar{X}$). From the peaks in the momentum distribution curve (MDC) at E_F (Fig. 2D), we can resolve the Fermi crossings of the bands contributing to the FS. Clearly, the two Fermi pockets near ± 0.4 Å^{-1} are electron pockets (e1) while the other four are hole pockets (h1 and h2). The band structures along cut #3 and cut #4 confirm that there are two hole-like bands and one-electron like band crossing E_F in each half of the BZ (Fig. 2F, G). Therefore, the observed overall size of hole pockets is almost twice of electron pockets (Fig. 2B), excluding a simple carrier compensation on the $\bar{\Gamma}$-$\bar{X}$-$\bar{Y}$ plane. Nevertheless, a perfect carrier compensation may still be established if the k_z dispersion of the energy bands is taken into account (see Supplementary Information for details), which will play a decisive role in the non-saturating magneto-resistance in T_d-WTe_2 (Ref. 2).

Temperature induced Lifshitz transition

Figure 3A illustrates the 3D plot of the electronic structure of T_d-WTe_2 at 82 K. While the band dispersions remain strongly anisotropic, there is clear variation in the size of Fermi pockets with

temperature. Upon increasing temperature, the electron pockets at $k_y = \pm 0.4$ Å^{-1} enlarge while the hole pockets at $k_y = \pm 0.2$ Å^{-1} shrink and become blurred, which indicates an upward shift of E_F (Fig. 3B(i)-(v)). Consistently, we observe systematic shift of energy bands at high binding energies as shown in Fig. 3C, D**.** The band top of the Γ_3 and Γ_2 bands sink down E_F near 90 K (Fig. 3C(iii)) and 220 K (Fig. 3B(vi) and Fig. 3E), respectively, suggesting the subsequent disappearance of the h1and h2 pockets on the FS and a temperature-induced two-stage Lifshitz transition in T_d-WTe_2.

Notably, in our *ab-inito* calculation, there exists a surface state (SS) connecting the hole band and the bottom of the electron band (SS in Fig. 2C(ii)). We found that due to its surface nature, the SS is sensitive to the surface condition and strongly depends on the sample cleavage[29]. As shown in Fig. 3F, G, the SS is clearly observed on the sample surface cleaved at 82 K, in good agreement with our *ab-initio* calculation in Fig. 2C(ii). The SS contributes a Fermi contour connecting the electron and hole pockets on the FS (Fig. 3G), which was regarded as intimately related to the TWS phase in T_d-$X$$Te_2$[25, 26, 28, 29].

Surface-modification induced Lifshitz transition

Since the surface electronic structure of T_d-WTe_2 strongly depends on the surface condition and the Weyl points reside above E_F of the pristine crystal (Fig. 1F), we investigated the evolution of the electronic structure of T_d-WTe_2 with the surface modification by systematic *in-situ* K dosing. The absorption of K atoms is monitored by the characteristic K 3*p* peaks in the core level photoemission spectra (Fig. 4A). With increasing K dosing time, the electron (hole) pockets on the FS shrink (enlarge) as shown in Fig. 4B. Consistently, the band dispersions along $\bar{Y}$-$\bar{\Gamma}$-$\bar{Y}$ shift towards high binding energies gradually. Resembling the evolution of the band structure with temperature, band top of the Γ_3 and Γ_2 bands sink down E_F after K dosing for 810 s and 2190 s, respectively, suggesting a two-stage Lifschitz transition induced by surface modification (Fig. 4B,C).

As summarized in Fig. 4D, E_F can be tuned upward for as large as 90 meV, allowing the approaching to both W1 and W2 in T_d-WTe_2. Unfortunately, the length of Fermi arc is too short (less than 1% of the BZ) to be resolved in our experiment. Yet, we note that the above-mentioned SS emerges with surface dosing and contributes a surface Fermi contour connecting the electron and hole pockets on the FS (Fig. 4B(iv-vi), 4C(iv-vi)), which is better resolved in the zoom-in plot of the band structure near k_x = 0.025 Å^{-1} after K dosing for 810 s (dashed curve in Fig. 4E). The emergence of the SS suggests the switch of the surface condition by K dosing, which might allude to a possible manipulation of the surface Fermi arc topology of the type-II TWS and calls for further investigation[33].

Visualization of strong spin-orbit coupling

Interestingly, after significant K dosing on the surface, the band structure shows a dramatic reconstruction, which is dominated by two cross-shape features near the $\bar{\Gamma}$ point (Fig. 4F) and resembles to the commonly observed surface Rashba splitting on alkali atoms deposited surfaces[34]. Indeed, our *ab-initio* calculation well reproduces these X-shape features by modelling the system with T_d-WTe_2 covered by a layer of K atoms (Fig. 4G), which suggests that the X-shape features are due to the surface Rashba effect. The Rashba parameters for X1 is about 0.18 eV Å, comparable with the normal Rashba splitting on metal surfaces. Notably, the X1 features a momentum offset as large as 0.16 Å^{-1}, which records the largest momentum offset of Rashba splitting to our knowledge[35]. The Rashba parameter for X2, on the other hand, is about 0.85 eV Å, which is much larger than that on the metal surfaces and comparable with surface enhanced Rashba effect on the surface alloy systems[35].

Discussion

T_d-phase transition metal dichalcogenides (T_d-WTe_2 and T_d-$MoTe_2$) share common properties and electronic structures as compared in the Supplementary Information. While the type-II TWS phase has been experimentally verified in T_d-$MoTe_2$, a direct observation of the characteristic surface

fermi arc in T_d-WTe_2 is still essentially lacking due to the extremely short Fermi arc (comparable with the momentum resolution). We emphasize that our measured band structure can be better reproduced by our *ab-initio* calculations (see Supplementary file for details) under reduced lattice parameter, which suggests a type-II TWS phase in T_d-WTe_2. Yet, in order to provide smoking-gun evidence for the type-II TWS phase, it is important to lengthen the Fermi arc. It is well-known that the Fermi arc in T_d-WTe_2 can be extended by Mo doping. The observed lattice contraction at low temperature (Fig. 1B) provides another way to substantially lengthen the Fermi arc according to our *ab-initio* calculations, which is instructive and incentive for the design and manipulation of the type-II TWS phase in T_d-WTe_2 via, e. g., temperature regulation and/or application of strain by fabricating ultra-thin films of T_d-WTe_2 on proper substrates.

On the other hand, the established two-stage Lifshitz transitions induced by temperature regulation and surface modification provide a feasible method to manipulate the electronic structure of T_d-WTe_2. Nevertheless, the mechanism for a temperature induced Lifshitz transition or substantial E_F shift is still intricate. We argue that both the unique electronic structure and lattice thermal expansion should play important roles. The hole like bands form a saddle point near the $\bar{\Gamma}$ point (Fig. 2C, E), which results in a large density of states (DOS) near E_F. With increasing temperature, the lattice expansion will provoke a dramatic reconstruction of the electronic structure and change of the DOS near E_F (Fig. 3C), which itself has to adjust in order to keep the charge neutrality.

Finally, we directly visualized the effect of the strong spin-orbit coupling effect in T_d-WTe_2 and establish a dramatic evolution of its electronic structure. These findings will not only help understand the puzzling extremely large and non-saturating magnetoresistance in T_d-WTe_2 and predicted quantum spin Hall effect in the monolayer limit (Ref. 2), but also promise many application potentials in electronic and spintronic devices.

Materials and Methods:

Materials:

High-quality single crystal T_d-WTe_2 was synthesized by the chemical vapor transport method with $TeCl_4$ as the transport additive. Polycrystalline T_d-WTe_2 was first obtained by solid reaction of high-purity (99.999%) W and Te powders in an evacuated quartz tube at 700°C for 1 week. 1g polycrystalline WTe2 and $TeCl_4$ (3 mg/ml) were then mixed, thoroughly grounded and sealed in an evacuated quartz tube which was heated in a two-zone furnace with a temperature gradient from 1,000 to 900 °C for another week. Black shining pallet with typical size of $2\times1\times0.1mm^3$ were obtained.

Angle resolved photoemission spectroscopy:

ARPES measurements were performed at beamline 10.0.1 of the Advanced Light Source (ALS) at Lawrence Berkeley National Laboratory, USA and BL I05 of the Diamond Light Source (DLS), UK. The measurement pressure was kept below 3×10^{-11} Torr at ALS and 9×10^{-11} Torr at DLS, and data were recorded by Scienta R4000 analyzers. The total convolved energy and angle resolutions were 16 meV and 0.2°, respectively. The fresh surface of T_d-WTe_2 for ARPES measurements was obtained by cleaving the high quality single crystals *in situ* along (001) cleavage plane. The surface dosing was conducted *in situ* by evaporating K atoms directly onto the cleaved sample surface at low temperature.

DFT calculations:

The electronic structure of T_d-WTe_2 was calculated by the density-functional theory (DFT) method implemented in the Vienna *ab-initio* Simulation Package (VASP). The exchange and correlation energy was considered in the generalized gradient approximation (GGA) with Perdew-Burke-Ernzerhof (PBE) based density functional and the spin-orbital coupling (SOC) was included self-consistently. The energy cut off was set to be 300 eV for the plane-wave basis. The tight binding matrix elements were calculated by projecting the Bloch wave functions to maximally localized

Wannier functions (MLWFs)[36]. The surface states were calculated from the half-infinite model by using the interative Green's function method[24]. K doped sample surface was simulated in a slab model by putting a layer of K atoms on the top surface of T_d-WTe_2, where the thickness of the slab is 7 unit cells.

Supplementary Materials

SI A: Photon energy dependent measurements on the electronic structure of T_d-WTe_2;

SI B: Polarization dependence of the electronic structure of T_d-WTe_2;

SI C: *ab-initio* calculation of the TWS phase in T_d-WTe_2;

SI D: Comparison between the TWS phases in T_d-WTe_2 and T_d-$MoTe_2$.

Fig. S1. k_Z dependence of the electronic structure of T_d-WTe_2.

Fig. S2. Polarization dependence of the electronic structure of T_d-WTe_2.

Fig. S3. Calculation of the type-II TWS phase in T_d-WTe_2.

Fig. S4. Comparison of the type-II TWS phase in T_d-WTe_2 and T_d-$MoTe_2$.

References and Notes

1. Qian, X., Liu, J., Fu, L. & Li, J. Quantum spin Hall effect in two-dimensional transition metal dichalcogenides. *Science* **346,** 1344-1347 (2014).
2. Ali, M. N. *et al.* Large, non-saturating magnetoresistance in WTe_2. *Nature* **514,** 205-208 (2014).
3. Wu, Y. *et al.* Temperature-Induced Lifshitz Transition in WTe_2. *Phys. Rev. Lett.* **115,** 166602 (2015).
4. Soluyanov, A. A. *et al.* Type-II Weyl semimetals. *Nature* **527,** 495-498 (2015).
5. Sun, Y. *et al.* Prediction of Weyl semimetal in orthorhombic $MoTe_2$. *Physical Review B* **92,** 161107 (2015).

6. Chang, T.-R. *et al.* Prediction of an arc-tunable Weyl Fermion metallic state in $Mo_xW_{1-x}Te_2$. *Nat Commun* **7,** (2016).
7. Wang, Z. *et al.* $MoTe_2$: Weyl and Line Node Topological Metal. *arXiv:1511.07440* (2015).
8. Wan, X., Turner, A. M., Vishwanath, A. & Savrasov, S. Y. Topological semimetal and Fermi-arc surface states in the electronic structure of pyrochlore iridates. *Physical Review B* **83,** 205101 (2011).
9. Burkov, A. A. & Balents, L. Weyl Semimetal in a Topological Insulator Multilayer. *Phys. Rev. Lett.* **107,** 127205 (2011).
10. Singh, B. *et al.* Topological electronic structure and Weyl semimetal in the $TlBiSe_2$ class of semiconductors. *Physical Review B* **86,** 115208 (2012).
11. Xu, G. *et al.* Chern Semimetal and the Quantized Anomalous Hall Effect in $HgCr_2Se_4$. *Phys. Rev. Lett.* **107,** 186806 (2011).
12. Hirayama, M. *et al.* Weyl Node and Spin Texture in Trigonal Tellurium and Selenium. *Phys. Rev. Lett.* **114,** 206401 (2015).
13. Liu, J. & Vanderbilt, D. Weyl semimetals from noncentrosymmetric topological insulators. *Physical Review B* **90,** 155316 (2014).
14. Hosur, P. Friedel oscillations due to Fermi arcs in Weyl semimetals. *Physical Review B* **86,** 195102 (2012).
15. Ashby, P. E. C. & Carbotte, J. P. Magneto-optical conductivity of Weyl semimetals. *Physical Review B* **87,** 245131 (2013).
16. Landsteiner, K. Anomalous transport of Weyl fermions in Weyl semimetals. *Physical Review B* **89,** 075124 (2014).

17. Weng, H. *et al.* Weyl Semimetal Phase in Noncentrosymmetric Transition-Metal Monophosphides. *Physical Review X* **5,** 011029 (2015).

18. Huang, S.-M. *et al.* A Weyl Fermion semimetal with surface Fermi arcs in the transition metal monopnictide TaAs class. *Nat Commun* **6,** (2015).

19. Xu, S.-Y. *et al.* Discovery of a Weyl fermion semimetal and topological Fermi arcs. *Science* **349,** 613-617 (2015).

20. Lv, B. Q. *et al.* Experimental Discovery of Weyl Semimetal TaAs. *Physical Review X* **5,** 031013 (2015).

21. Yang, L. X. *et al.* Weyl semimetal phase in the non-centrosymmetric compound TaAs. *Nature Phys.* **11,** 728-732 (2015).

22. Liu, Z. K. *et al.* Evolution of the Fermi surface of Weyl semimetals in the transition metal pnictide family. *Nat Mater* **15,** 27-31 (2016).

23. Deng, K. *et al.* Experimental observation of topological Fermi arcs in type-II Weyl semimetal $MoTe_2$. *arXiv:1603.08508* (2016).

24. Jiang, J. *et al.* Observation of the Type-II Weyl Semimetal Phase in $MoTe_2$. *arXiv:1604.00139* (2016).

25. Liang, A. *et al.* Electronic Evidence for Type II Weyl Semimetal State in $MoTe_2$. *arXiv:1604.01706* (2016).

26. Xu, N. *et al.* Discovery of Weyl semimetal state violating Lorentz invariance in $MoTe_2$. *arXiv:1604.02116* (2016).

27. Huang, L. *et al.* Spectroscopic evidence for type II Weyl semimetal state in $MoTe_2$. *arXiv:1603.06482* (2016).

28. Wang, C. *et al.* Spectroscopic Evidence of Type II Weyl Semimetal State in WTe2. *arXiv:1604.04218* (2016).
29. Bruno, F. Y. *et al.* Surface states and bulk electronic structure in the candidate type-II Weyl semimetal WTe_2. *arXiv:1604.02411* (2016).
30. Jiang, J. *et al.* Signature of Strong Spin-Orbital Coupling in the Large Nonsaturating Magnetoresistance Material ${\mathrm{WTe}}_{2}$. *Phys. Rev. Lett.* **115,** 166601 (2015).
31. Tamai, A. *et al.* Fermi arcs and their topological character in the candidate type-II Weyl semimetal $MoTe_2$. *arXiv:1604.08228* (2016).
32. Pletikosić, I. *et al.* Electronic Structure Basis for the Extraordinary Magnetoresistance in WTe_2. *Phys. Rev. Lett.* **113,** 216601 (2014).
33. Sun, Y., Wu, S.-C. & Yan, B. Topological surface states and Fermi arcs of the noncentrosymmetric Weyl semimetals TaAs, TaP, NbAs, and NbP. *Physical Review B* **92,** 115428 (2015).
34. King, P. D. C. *et al.* Large Tunable Rashba Spin Splitting of a Two-Dimensional Electron Gas in Bi_2Se_3. *Phys. Rev. Lett.* **107,** 096802 (2011).
35. Ishizaka, K. *et al.* Giant Rashba-type spin splitting in bulk BiTeI. *Nat Mater* **10,** 521-526 (2011).
36. Mostofi, A. A. *et al.* wannier90: A tool for obtaining maximally-localised Wannier functions. *Computer Physics Communications* **178,** 685-699 (2008).

Acknowledgments

Funding: This work is supported by the EPSRC Platform Grant (Grant No.EP/M020517/1), Hefei Science Center CAS (2015HSC-UE013), the ERC Advanced Grant (No. 291472), the NRF,

Korea through the SRC center for Topological Matter (No. 2011-0030787) and the Bureau of Frontier Sciences and Education, Chinese Academy of Sciences.

Author contributions: Y.L.C. conceived the experiments. ARPES measurements were performed by L.X. Y. and Z.K.L. with support from H.F.Y., J.J., S.K.M. and Z.H. DFT calculations were conducted by Y.S., X.F.Q., L.F. and B.H.Y. Single crystals were grown and characterized by S.H.Y., M.H.L. and C.F. Data analysis and manuscript preparation were done by L.X.Y., Z.K.L. and Y.L.C., with input from all authors.

Competing interests: The authors declare no competing financial interests.

Figures and Tables

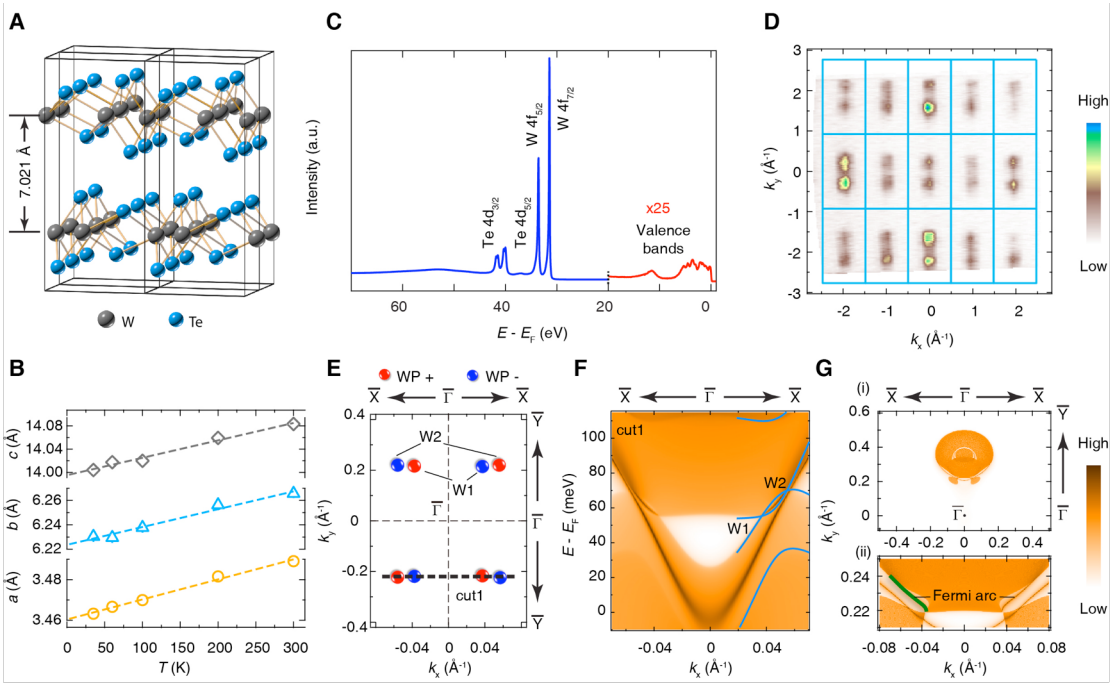

Fig. 1. Basic characterization of T_d-WTe_2. **(A)** The quasi-1D crystal structure of T_d-WTe_2. The W atoms form zigzag chains in the b direction and the flat Te layers winkles to compensate the lattice distortion. **(B)** The lattice constants of WTe_2 as a function of temperature. **(C)** Core level photoemission spectrum of WTe_2 showing characteristic Te 4d and W 4f peaks. **(D)** Fermi surface in multiple BZs showing the quasi-1D fermiology of T_d-WTe_2. **(E)** The predicted locations of Weyl points (WP) in the projected surface BZ. The Weyl points with different chirality is indicated by different colors. **(F)** The calculated band structure of T_d-WTe_2 near the Weyl points along cut #1 as marked in panel **e**. The solid blue curves are the calculated bulk bands. **(G)** (i),Calculated constant energy contour of WTe2 at 55 meV above the Fermi energy (E_F). (ii), The zoom-in plot shows the surface Fermi arc (green curve) connecting the electron and hole pockets.

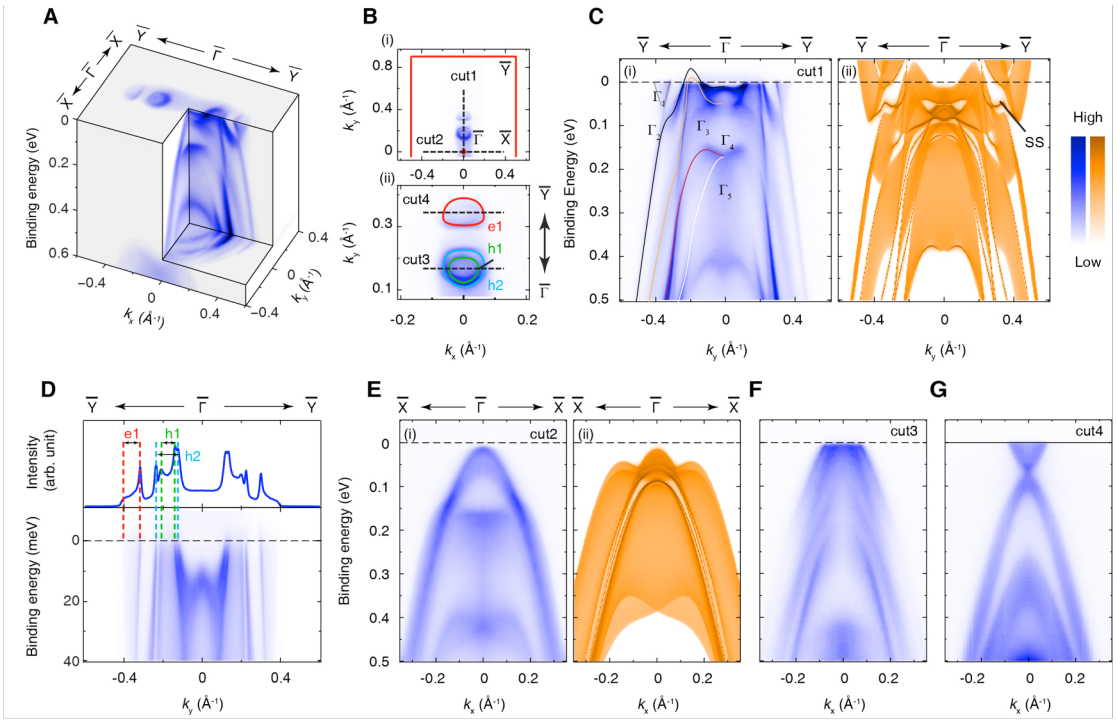

Fig. 2. Band structure along high symmetric directions and Fermi surface (FS) map at 9 K. (A) 3D illustration of the band structure of WTe2. **(B)** (i),Fermi surface map in the first BZ. The red lines indicates the surface BZ. (ii), The zoom-in plot of the FS. The colored curves are the guides to the eyes for the Fermi pockets. The black dashed lines marks different measurement directions. **(C)** The compassion of the measured (i) and calculated (ii) band structure along the $\bar{Y}$-$\bar{\Gamma}$-$\bar{Y}$ direction. The solid curves are the guides to the eyes for the band dispersions. **(D)** The zoom-in plot of the dispersion near the E_F showing the Fermi crossings of the hole and electron pockets together with the momentum distribution curve at E_F. **(E)** The comparison of the measured (i) and calculated (ii) band structure along the $\bar{X}$-$\bar{\Gamma}$-$\bar{X}$ direction. **(F, G)** Band structures along cuts #3 and #4 as marked in panel B.

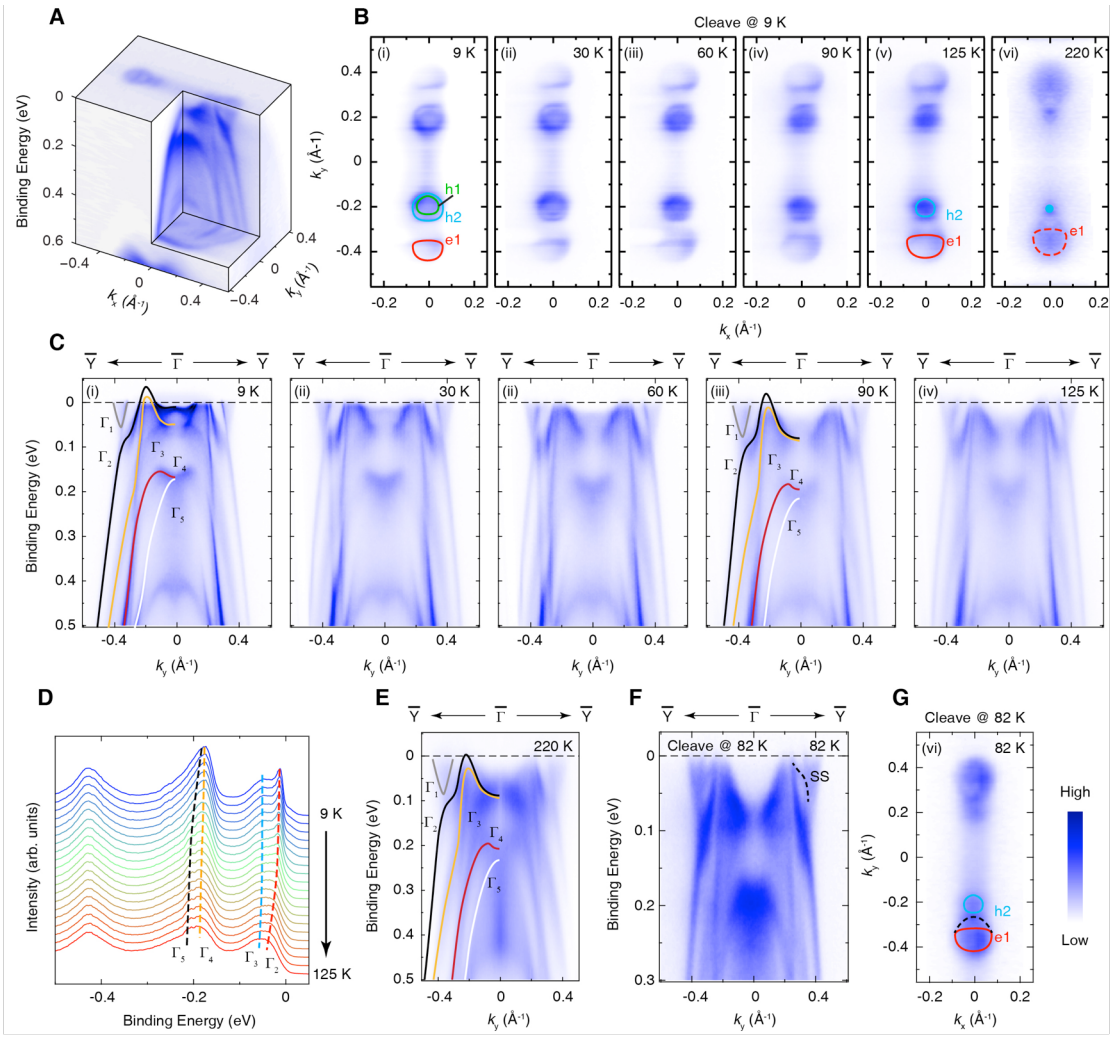

Fig. 3. Evolution of the band structure of T_d-WTe_2 with temperature. **(A)** 3D illustration of the band structure of WTe2 at 82 K. **(B)** The evolution of the Fermi surface with temperature. **(C)** The evolution of the band structure along the $\bar{Y}$-$\bar{\Gamma}$-$\bar{Y}$ direction with increasing temperature. **(D)** The evolution of the EDC near the $\bar{\Gamma}$ point with increasing temperature. The colored dashed curves are the guides to the eyes for the shift of the bands. **(E)** The band structure near E_F at 220 K. **(F)** The observation of the surface state on a sample surface cleaved at 82 K. **(G)** The FS obtained on a sample surface cleaved at 82 K. The ss contributes a Fermi contour connecting the hole and electron pockets (black dashed curve).

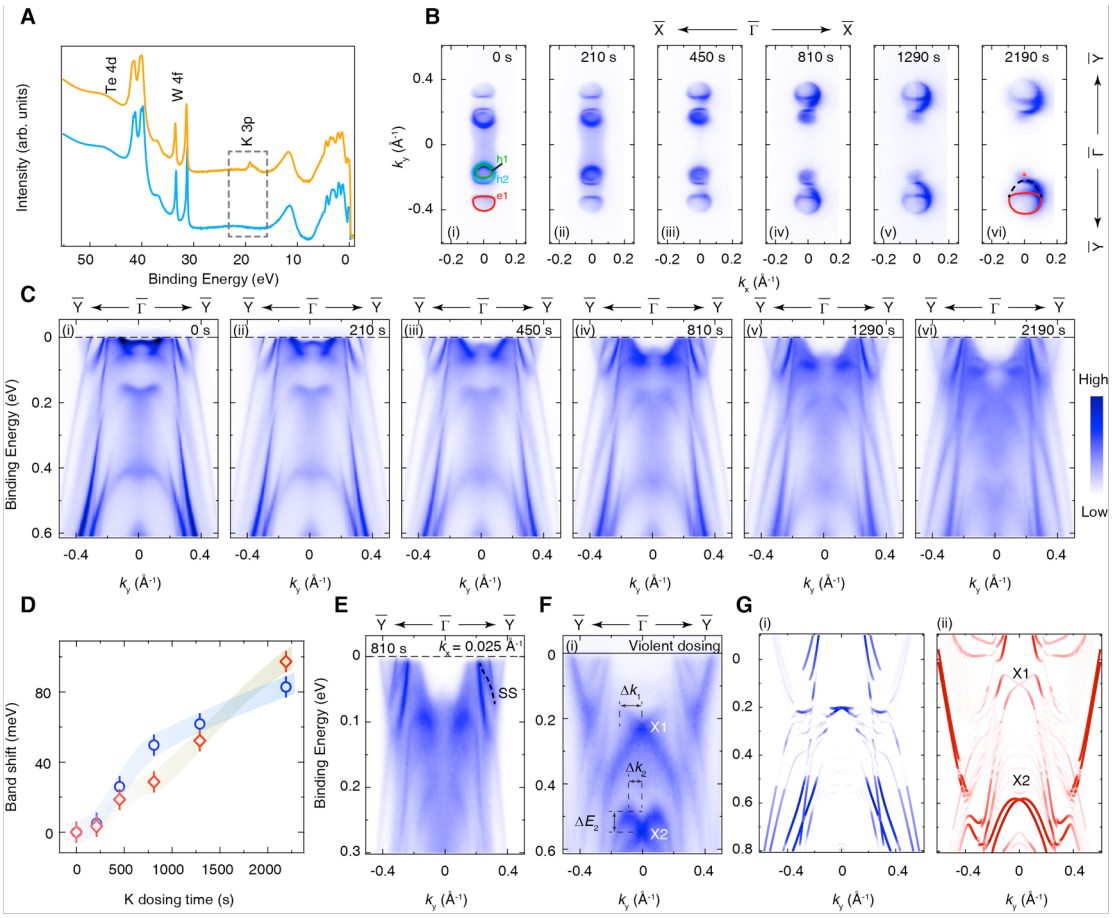

Fig. 4. Band evolution with surface modification. (**A**) The photoemission core level spectra with characteristic W, Te and K peaks before (blue) and after (orange) potassium dosing. **(B)** The evolution of the Fermi surface of WTe_2 with potassium dosing. **(C)** The evolution of the band structure along the $\bar{Y}$-$\bar{\Gamma}$-$\bar{Y}$ direction with K dosing. **(D)** The summarized band shift as a function of surface dosing time. **(E)** The zoom-in plot of the band dispersion along the $\bar{Y}$-$\bar{\Gamma}$-$\bar{Y}$ direction at $k_x = 0.025$ Å^{-1}. **(F)** The band structure of K dosed WTe_2 after significant surface dosing. Two prominent X-shape features (X1 and X2) were observed. **(G)** The calculated band structure on the pristine (i) and K-dosed (ii) surface. X1 and X2 were well reproduced by the theoretical calculation.